Journal of Fluorescence, Vol. 7, No. 1, 1997

Construction and Characterization of a Frequency-Domain Fluorescence Lifetime Imaging Microscopy System

Theodorus W. J. Gadella, Jr.,[1,3] Arie van Hoek,[2] and Antonie J. W. G. Visser[1]

Received June 14, 1996; accepted September 26, 1996

The construction of a homodyne frequency domain fluorescence lifetime imaging microscope is described. The system consists of (i) an intensity-modulated laser excitation source, (ii) an epifluorescence microscope, (iii) a gain-modulated microchannel plate (MCP) image intensifier, and (iv) a slow-scan CCD camera. The phase and modulation homogeneity of the MCP image intensifier were determined at frequencies of 40, 100, 160, and 240 MHz. The detected modulation depths were 65, 52, 32, and 23%, respectively, and were highly homogeneously distributed. The phase-distribution image revealed iris effects at frequencies of 160 and 240 MHz but was homogeneous at lower frequencies. Lifetime imaging of a solution of the fluorescent flavoprotein lipoamide dehydrogenase demonstrated (i) the accuracy of the determined lifetimes (<60 ps), (ii) the time resolution of the instrument (<50 ps), and (iii) the average precision for single pixel fluorescence lifetimes (50 ps is feasible). The imaging of tiny fluorescent microspheres revealed that even in a volume of 0.3×10^{-15} L, the standard error in the lifetimes can be as low as 79 ps. The spatial resolution of the instrument is estimated to be <400 nm in the object plane at a 100× magnification.

KEY WORDS: Time-resolved fluorescence; image intensifier; modulation; image processing.

INTRODUCTION

Fluorescence lifetime imaging microscopy, the spatially resolved detection of fluorescence lifetimes in a microscopic specimen, adds the nanosecond time dimension to conventional fluorescence microscopy. The utilization of this time dimension enables numerous novel imaging applications, which are particularly useful in the field of cell biology. The application of FLIM for quantitative microscopy,[1] for achieving new methods of image contrast in tumor imaging,[2] for imaging of cellular parameters such as pH,[3] oxygen,[4] and Ca^{2+} concentration,[5,6] and for detecting spatially resolved FRET efficiencies revealing *in situ* molecular interactions[7] have been described (see also other papers in this issue). As in the spectroscopy counterpart, FLIM can be implemented in the time domain using pulsed excitation light or in the frequency domain using intensity-modulated excitation light. Starting in 1989, several papers have been published from different laboratories that report on the construction of functional two-dimensional imaging FLIM systems employing either the time-domain approach[8–15] or the frequency-domain approach.[16–22] Both approaches have also been incorporated in confocal fluorescence microscope systems.[12,22] Interestingly, one generation earlier (in 1958), Benjamin Venetta constructed a (nonimaging) frequency domain time-resolved fluorescence microscopy system, and hence he can be regarded as the pioneer in the field.[23] Recently, a two-photon frequency domain FLIM system with superior *z*-

[1] MicroSpectroscopy Center (MSC) Wageningen, Department of Biochemistry, Wageningen Agricultural University, The Netherlands.
[2] MSC Wageningen, Department of Molecular Physics, Wageningen Agricultural University, Wageningen, The Netherlands.
[3] To whom correspondence should be addressed: MSC Wageningen, Department of Molecular Biology, Wageningen Agricultural University, Dreijenlaan 3, NL-6703 HA Wageningen, The Netherlands.

1053-0509/97/0300-0035$12.50/0

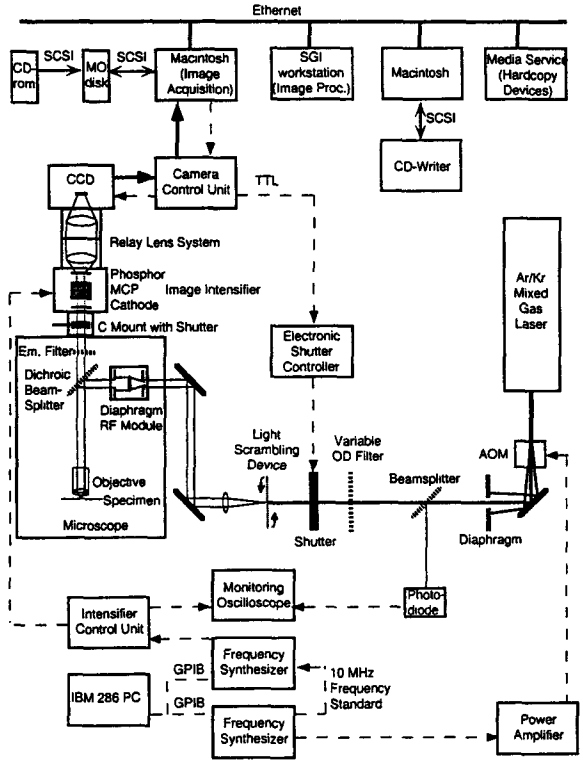

Fig. 1. *Schematic representation of the frequency-domain fluorescence lifetime imaging microscope.* The dashed lines indicate triggering or (RF) control signals. For details see text.

axis resolution has been constructed at the Laboratory for Fluorescence Dynamics (LFD).[24] FLIM systems have been reviewed in Refs. 20 and 25–27.

The experimental methodology of measuring lifetime-resolved fluorescence microscopic images in the frequency domain is based on the technique of phase fluorometry.[28,29] Upon excitation of a microscopic sample with intensity-modulated light, the fluorescence emission will also be intensity-modulated at an identical frequency. The phase and modulation of the fluorescence emission relative to the excitation light carry information from which the fluorescence lifetimes can be calculated. Given (i) the detection of the intensity-modulated fluorescence emission at a frequency f; (ii) a phase delay of the fluorescence emission relative to excitation light of $\Delta\Phi$ degrees; and (iii) a modulation (defined as the AC signal divided by the DC signal) of the emission (M_F) relative to that of excitation light (M_E) of M ($= M_F/M_E$), then two equations relate these experimentally determinable parameters to average lifetimes τ_Φ and τ_M. In their turn, these average lifetimes are directly related to the K decaying fluorescence components with fluorescence lifetime τ_k and relative amplitude a_k in the time domain [see Eqs. (1) and (2)].[28–30] When there is a single exponential decay ($K = 1$), $\tau_\Phi = \tau_M = \tau_1$. In the case of a multicomponent decay ($K > 1$), generally $\tau_\Phi < \tau_M$, allowing a simple and effective discrimination between single- and multicomponent fluorescence decays. For a detailed mathematical treatment of frequency domain FLIM we refer to Ref. 31, but see also Refs. 27, 32, and 33.

$$\tau_\Phi = \frac{1}{2\pi f}\tan\Delta\Phi = \sum_k^K \frac{a_k\tau_k^2}{1+(2\pi f\tau_k)^2} \Big/ \sum_k^K \frac{a_k\tau_k}{1+(2\pi f\tau_k)^2} \quad (1)$$

$$\tau_M = \frac{1}{2\pi f}\sqrt{\frac{1}{M^2}-1} = \quad (2)$$

$$\frac{1}{2\pi f}\left\{\left(\sum_k^K a_k\tau_k\right)^2 \Big/ \left[\left(\sum_k^K \frac{2\pi f a_k\tau_k^2}{1+(2\pi f\tau_k)^2}\right)^2 + \left(\sum_k^K \frac{a_k\tau_k}{1+(2\pi f\tau_k)^2}\right)^2\right] - 1\right\}^{1/2}$$

In this paper, we describe in detail the construction of a frequency-domain FLIM system in our laboratory using the homodyne technique of detection. In the instrument, the fluorescence lifetimes are measured by spatially resolved detection of $\Delta\Phi$ and M [Eqs. (1) and (2)], which is achieved by means of incorporation of a radio frequency (RF) gain-modulated image intensifier in the emission pathway of a fluorescence microscope.[21,25,31,33] Instrument performance characteristics such as attainable accuracy, time resolution, and spatial resolution are discussed.

INSTRUMENTAL

FLIM Hardware

The complete FLIM setup (see Fig. 1) was placed on an optical table (1.2 × 2 m; Technical Manufacturing Corporation, Peabody, MA) with a rigid honeycomb body structure and a stainless-steel top with mounting holes for the optical components. For microtranslation and mounting, different optical components from Spindler & Hoyer (Göttingen, Germany) and from Newport Corporation (Irvine, CA) were used.

Frequency and Phase Control. For frequency-domain FLIM, it is required to control independently the frequency and/or relative phase of the modulation of the excitation light and the (fluorescence emission) detector gain. Hence, our microscope system incorporated two frequency synthesizers, both with a frequency range of 0.1–310 MHz (resolution, 0.1 Hz) and a relative phase range of 0–360° (resolution, 0.225°) (Model PTS 310, Programmable Test Sources, Littleton, MA). To achieve highly stable relative phase settings between the synthesizers (essential for the homodyne mode of operation),

a common crystal reference (Model OCXO; stability, 3 $\times$ 10^{-9}/day) was used, enabling a higher phase stability than the conventional phase locking as described by others.[27,33,34] The synthesizers were controlled independently by means of GPIB interfacing to an IBM 286PC, using a PCL-848 A/B multifunction IEEE-488 interface card (Advantech Corp. Ltd., Taipei, Taiwan) and home-written programs in GW-Basic (DOS).

Excitation. One of the many laser lines (range, 458–676 nm) from an Innova 70 Spectrum Ar/Kr mixed gas laser (Coherent, Santa Clara, CA) was selected for excitation. Two acoustooptic modulators (AOMs; Dr. A. Barocsi, Department of Atomic Physics, Technical University of Budapest, Hungary), one with a frequency band from 20 to 40 MHz, the other from 50 to 100 MHz, could be used. Within these frequency bands, one of the peaks out of a comb of sharp acoustic resonances was selected to get a deep modulation of the light. To obtain intensity-modulated laser light at a RF frequency f (range, 10–120 MHz), one of the AOMs was driven at $^1/_2f$ by one of the PTS 310 signal generators coupled to a power amplifier (0.5–50 MHz, 1 W; Dr. A. Barocsi, Department of Atomic Physics, Technical University of Budapest). Either the zero- or the first-order diffraction spot was selected by using diaphragms in the light path. The modulation quality was monitored continuously using a PIN photodiode at -24V reverse bias (Model 5082-4203; Hewlett Packard, Palo Alto, CA) and an oscilloscope (Model 2252; Tektronix, Beaverton, OR). To minimize local excitation intensity fluctuations in the specimen due to interference (speckle) of the coherent laser light, the excitation beam was hitting a rotating ($\approx$10-Hz) scattering object (Scotch Magic 810 tape) and the scattered light was recollimated by a lens (focal length, 5 cm) and directed towards the back entrance of the fluorescence microscope by means of a pair of mirrors. A fast electronic shutter (Model Uniblitz LS 6 with T132 driver; Vincent Associates, Rochester, NY) was placed in the excitation light path and could be controlled manually or synchronously with the CCD-camera shutter.

Microscope. The fluorescence microscope (Leica DMR-BE; Leitz, Wetzlar, Germany) was equipped with a Leica Diaphragm RF Module (incorporating a field and intensity iris diaphragm) and with several microscope objectives and fluorescence filter cubes. For the experiments described here, we used the PL Fluotar 10$\times$ NA 0.3 air and the PL Fluotar 100$\times$ NA 1.3 oil objectives and the fluorescence filter cube containing only a 505-nm DRLP dichroic mirror (Omega Optical, Inc., Brattleboro, VT). Furthermore, a GG 515 (Schott, Mainz, Germany) cutoff filter was inserted in the emission light path by means of a home-built filter holder positioned at the analyzer IC/P polarizer holder position of the microscope.

Image Intensifier. The image intensifier (Model C5825; Hamamatsu Photonics K.K., Toyooka-village, Shizuoka-ken, Japan) was connected to the phototube exit of the microscope by means of a home-built C-mount adapter incorporating a (manual) shutter for safety reasons (regarding the intensifier photocathode). The image intensifier was equipped with an S25 photocathode (ϕ, 17.5 mm), a two-stage MCP, and a P43 phosphor and enabled RF gain modulation (0.3–300 MHz with modulation depths up to 100%). The intensifier RF gain modulation was driven by a PTS 310 signal generator coupled to the intensifier control unit. The exact scheme of gain modulation of the image intensifier (patented by Hamamatsu) is unknown to the authors, but it appears that Hamamatsu found a way of modulating the photocathode at a relatively low voltage and impedance, giving rise to superior performance. The RF reference output of the control unit was monitored on the oscilloscope. The microscopic image was focused directly onto the photocathode of the image intensifier. The light emitted from the phosphor screen of the intensifier was passed onto the CCD camera using a relay lens set (Nikon models Nikkor 85/1.4 and Nikkor 105/1.8). The optical amplification (0.81$\times$) of this lens set was chosen to match the resolution of the image intensifier (>25 lp/mm) with the size of the pixels on the CCD.

CCD Camera. Images were captured by a slow-scan Series 200 (CH250) charge-coupled device (CCD) camera (Photometrics Ltd., Tucson, AZ, USA) system that consisted of (i) a thermoelectrically cooled SI 502/AB grade 1 thinned and back-illuminated CCD sensor with multiphase pinning (MPP) containing 510 $\times$ 510 (available) square 24-μm pixels, with a full well capacity of 376 ke^-, a dark current of 0.87 e^-/s at -40°C, and a quantum yield up to 80%; (ii) a liquid cooling circulator (LCU220) permitting standard cooling of the chip down to -40°C; (iii) a CE200a camera control unit with a built-in 14-bit (0–16,383) analog-to-digital converter operating at 200 kHz; (iv) a Nu200 interface card inserted into a Nubus slot of an Apple Macintosh PowerPC7100/66 16/500Mb computer; and (v) camera control software by the IPLab 3.0 program (Signal Analytics, Vienna, VA).

FLIM Operation

After taking a blank image (excitation shutter closed), 10 phase images (generally 0.1–2 s of exposure

to excitation light each) were collected by the CCD camera at different phase settings between the signal generators driving the AOM and the image intensifier (consecutive phase images differ by 36°, thereby covering one homodyne period). When photobleaching was suspected in the specimen, 10 additional images were acquired starting at a phase difference of 314° with −36° steps (ending at 0°). Photobleaching can be corrected for by using a nonlinear single-exponential fit to the ratio of the average intensities in the images taken at identical phase settings or, alternatively, by using a linear procedure, by digital addition of the intensities in the images taken at identical phase settings.[31,33] It is of note that the high detection efficiencies of this system require only very short exposure times to excitation light (0.1–2 s), thereby minimizing photobleaching. In the data presented here, photobleaching was <1%. The reference phase and modulation were obtained by monitoring scattered light (after removing the emission filter from the microscope and attenuation of the excitation light intensity by means of a variable neutral density filter, transmission 1–100%, positioned in the excitation light path).

Data Analysis and Image Processing

In a previous paper, the data analysis procedures were described in detail.[31] Data analysis was performed by stand-alone self-written computer programs (SINUS and SINUS2L) using a FORTRAN source code. Image processing of the image-file output from these programs was done using the TCL-Image program (TPD; Technical University of Delft, Delft, The Netherlands) implemented on a DEC MicroVax II computer.[25,31] In the current situation, the analysis routines (which have not changed) and image processing routines have been integrated and attached to the commercial image processing package SCIL-Image (TPD) which is running on a powerful Silicon Graphics Inc. (SGI) workstation. Prior to the attachment to the SCIL-Image, the original SINUS and SINUS2L FORTRAN source codes (with minor changes regarding data input-output routines) were translated into the C language by the public-domain FORTRAN-to-C translation tool f2c. As mentioned before,[31] due mainly to the improved computer hardware, the improvement in speed is over 20-fold in the new situation, yielding computation times of less than 100 μs/pixel.

The image processing routines that were implemented in TCL-image[31] had to be rewritten completely into C and are now fully integrated with the analysis routines in the SCIL-Image environment. In short, the image processing routines, currently implemented in SCIL-Image, add text to identify the different result images, make histograms of fluorescence intensities and fluorescence lifetimes, and make two-dimensional histograms depicting correlation between the fitted parameters in the images. By means of the user-friendly SCIL-Image command interface, the user is able to select several modes of output to his convenience. The final processed images can be exported as TIFF files which can be easily incorporated in several software packages on IBM PCs or Macintosh computers for further processing or incorporation into text documents.

For convenient storage of the large quantities of the image data, we used a rewritable 230-Mb magnetooptical disk drive (Model M2512A; Fujitsu Ltd., Tokyo) as data buffer and a CD writer (Philips CDD522, Eindhoven, The Netherlands) for final storage of the data on 630-Mbyte nonrewritable CD roms. Hardcopies on paper or transparencies (using a Fujix Pictrography 3000 printer, Fuji, Tokyo) and 35-mm slides were generated at the MediaService Department of our university.

RESULTS AND DISCUSSION

Performance Characteristics of the Image Intensifier

To investigate the performance characteristics of the image intensifier, we studied the modulation depth and the phase homogeneity at different frequencies using scattered excitation light. The results are summarized in Fig. 2. As inferred by Fig. 2, the modulation image is homogeneous at all frequencies. The actual detected modulation depths (defined as the AC component divided by the DC component of the fitted sine wave describing the experimental data) are above 0.5 (i.e., >50%) at 41.6 and 100.9 MHz. For the homodyne mode of operation, the detected modulation depth is equal to $^1/_2 M_E M_A$,[31] where M_E and M_A are the modulation depths of the excitation light and the detector gain, respectively. This indicates that the product of $M_E M_A$ is greater than 1. This is caused by a combination of a deep detector gain modulation and a pulse-shaped excitation light intensity modulation, giving rise to a modulation depth over 100% at the fundamental frequency. That indeed the excitation is pulse shaped at, for instance, 80.1 MHz is also clear from the fact that one can detect modulation at the first (160.2-MHz) and second (240.3-MHz) harmonic frequencies (see Fig. 2). It is of note that even at these frequencies detected modulation depths were as high as 32 and 23%, respectively. These very high modulation depths and

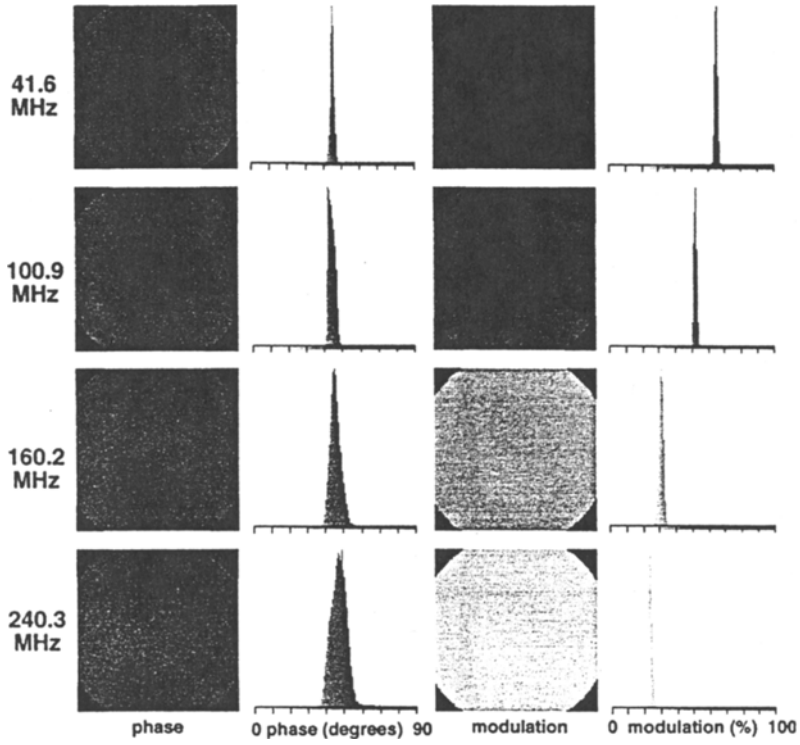

Fig. 2. *Homogeneity of relative phase and modulation of the microchannel plate image intensifier at various detector gain modulation frequencies.* All phase and modulation images were calculated from 10 phase images of scattered excitation light (476.5 nm) using the 10× objective, and 2 × 2 binning on the CCD, yielding 255 × 255 pixel-sized images. For the images at 41.6 MHz, the 20- to 40-MHz AOM was driven at 20.8 MHz, and the zero-order diffraction spot was selected. For the images at 100.9 MHz, the 50- to 100-MHz AOM was driven at 50.45 MHz, and the first-order diffraction spot was selected. For the images at 160.2 and 240.3 MHz, the 50- to 100-MHz AOM was driven at 40.05 MHz and the zero-order diffraction spot was selected. Hence the detector gain modulation was chosen so as to image the first and second harmonic of the fundamental 80.1-MHz excitation light modulation at the 160.2- and 240.3-MHz detector modulation frequencies, respectively.

modulation homogeneity even at frequencies up to 240 MHz allow a very accurate τ_M fluorescence lifetime determination.

The phase chosen for detection is of course arbitrary but was set to 45° for all experiments in Fig. 2 for comparative reasons. The homogeneity of phase is close to ideal at frequencies between 40 and 100 MHz, which is a convenient frequency range for detection of average fluorescence lifetimes in the range of 0.5–10 ns, thereby covering most of the known fluorescence probes. At 160 MHz and above, the phase homogeneity becomes progressively less. The spatial dependency of the phase at higher frequencies is an instrumental artifact known, as the iris effect. We note that the iris effect observed here is nearly absent below 100 MHz and still relatively insignificant at higher frequencies (i.e., compare the results published for another frequency-domain FLIM system[27]). From this we conclude that for a reference measurement at frequencies below 100 MHz, only the average image intensities of a reference phase image set need to be fitted to a sine wave, resulting in a considerably faster data analysis procedure.

Accuracy of Fluorescence Lifetimes Determined by FLIM

To illustrate the accuracy of our FLIM instrument, the results of a solution of the fluorescent flavoenzyme lipoamide dehydrogenase (LipDH) isolated from *Azotobacter vinelandii*[35,36] in potassium–phosphate buffer placed in a microcuvette are shown in Fig. 3. As is apparent from the original and calculated phase images, the observed data hardly deviate from a sinusoidal shape (see also difference images). This is also inferred from the image-averaged correlation coefficients (99.96%) and residuals (0.6%) of the fit. For definition of these constants we refer to Refs. 31 and 33. The image-averaged τ_Φ is 2.07 ns [coefficient of variation (CV), 2.3%] and τ_M = 2.09 ns (CV, 1.5%). These average fluorescence lifetimes compare favorably with the expected

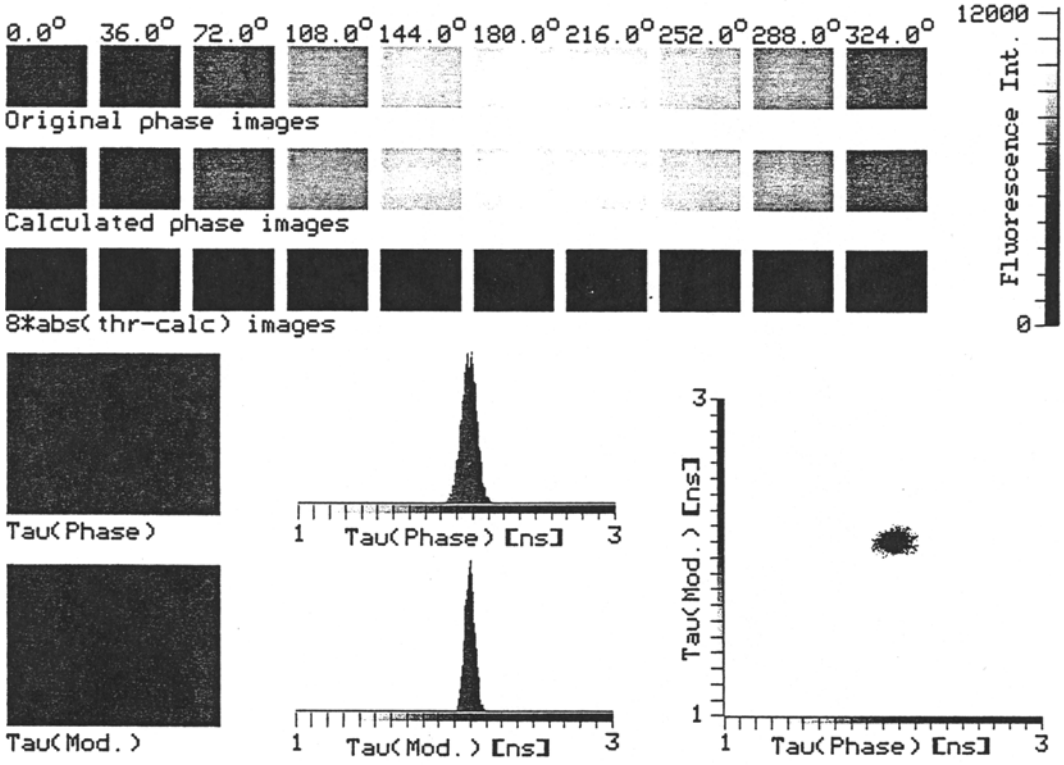

Fig. 3. *FLIM analysis of homogeneous solution of lipoamide dehydrogenase (LipDH).* LipDH (75 μ*M*) was dissolved in a 50 m*M* potassium phosphate buffer at pH 7.0 and placed in a microcuvette (cross section, 0.2 × 2 mm; Model 3520; VitroCom, Inc., Mountain Lakes, NJ) at room temperature. The sample was excited using the 476.5 laser line modulated at 100.9 MHz, using the 50- to 100-MHz AOM driven at 50.45 MHz, and the first-order diffraction spot was selected. After a blank image (excitation off), 10 phase images were recorded (0.5-s exposure time to excitation light each) using the 10× objective and 2 × 2 binning on the CCD. The first row of images shows the original phase-resolved images, the second row depicts the calculated phase images (based on the fitted phase and modulation at each individual pixel), and the third row depicts the absolute difference between the calculated and the original phase images multiplied by 8. The τ_Φ image and temporal histogram, the τ_M image and temporal histogram, and the two-dimensional histogram depicting the correlation between τ_Φ and τ_M are shown in the bottom half of the image.

lifetimes of 2.02 and 2.15 ns for τ_Φ and τ_M, respectively. These expected times were calculated from Eqs. (1) and (2) using $a_1 = 0.06$, $\tau_1 = 0.2$ ns, $a_2 = 0.31$, $\tau_2 = 1.4$ ns, $a_3 = 0.63$, and $\tau_3 = 2.4$ ns as determined by Bastiaens *et al.* with the time-resolved single-photon counting technique (utilizing the same buffer at 293 K[36]). For individual pixels, the average standard errors (due to noise) in τ_Φ and τ_M are 51 and 40 ps. It is of note that the image averaged residuals and coefficients of deviation are twofold lower and the average standard errors are four times lower than the best (and only) so far published for another FLIM system.[7,31] Hence, we conclude that with our FLIM instrument time resolutions of <50 ps, accuracies of <60 ps, and an average precision for each determined pixel of about 50 ps are feasible. In our opinion, each of these characteristics is unprecedented in the current FLIM literature.

Spatial Resolution

The spatial resolution of the FLIM system was investigated using fluorescent latex beads with a diameter of 5 μm. An extended fluorescence lifetime analysis of these tiny fluorescent particles is shown in Fig. 4. The lifetimes are very homogeneous in the fluorescent beads as is apparent from the constant gray value in the lifetime images τ_Φ and τ_M and the narrow lifetime distribution in the corresponding histograms. The average lifetimes of these beads are determined as $\tau_\Phi = 4.13$ ns (CV, 4.1%) and $\tau_M = 4.14$ ns (CV, 3.3%) and clearly demonstrate that accurate lifetimes can be determined in volumes of 65×10^{-15} L (the volume of one bead). The calculated true standard deviation in the fluorescence lifetimes in the specimen (i.e., corrected for standard errors for individual lifetime measurements; for definition see Ref. 31) is only 129 and 79 ps for τ_Φ and τ_M, re-

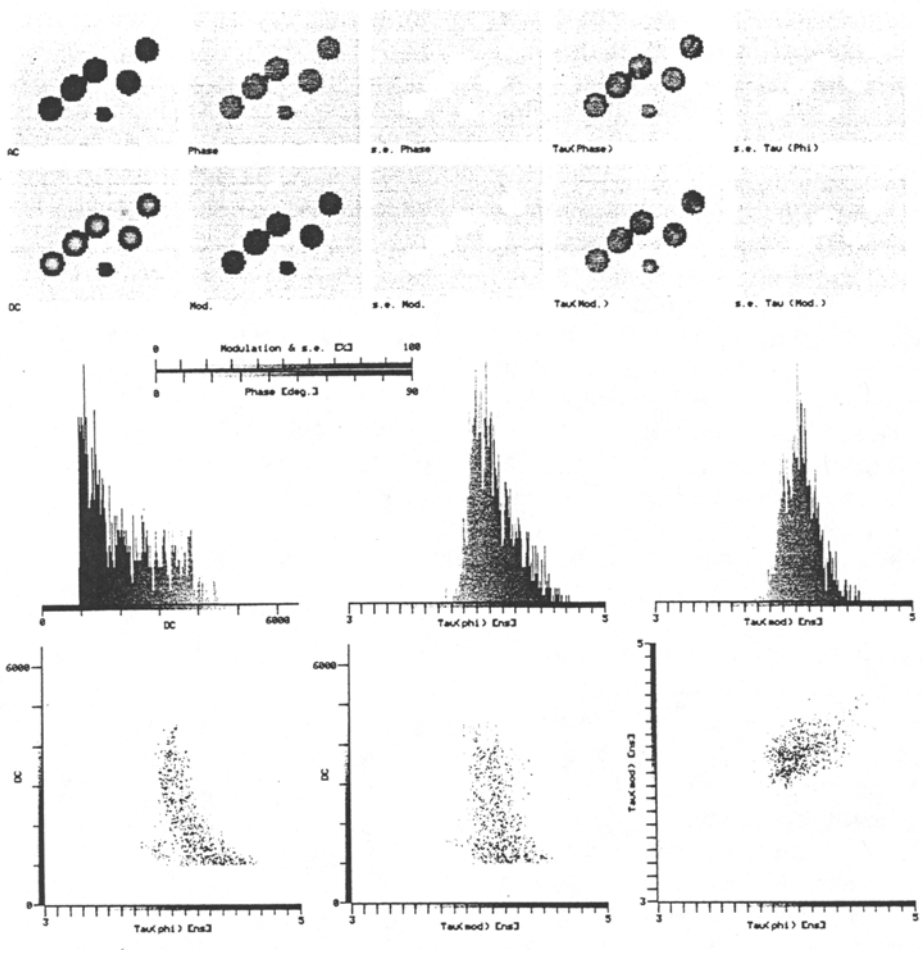

Fig. 4. *FLIM analysis of fluorescent microspheres.* Multispeck fluorescent microspheres (ϕ = 5 μm; Catalog No. M-7900; Molecular Probes, Inc., Eugene, OR) were excited with the 488-nm laser line modulated at 40.0 MHz, using the 20- to 40-MHz AOM driven at 20.0 MHz. The first-order diffraction spot was selected. After a blank image (excitation off), 10 phase images were recorded (1.0-s exposure time to excitation light each) using the 100× objective, a modulation of the image intensifier at 40.0 MHz, and a 1 × 1 binning on the CCD. The standard complex output of the image analysis and processing software shows the various images calculated from the fit in the first two rows, the DC fluorescence intensity histogram and the temporal histograms of τ_Φ and τ_M in the second row, and three two-dimensional histograms depicting the correlation between these parameters in the fourth row. The gray scale of the histograms corresponds to the gray values in the images in the top two rows. The phase, modulation, and relative standard error images (depicted with SE) have a scaling as indicated in the correspondingly labeled gray-value bar.

spectively, indicating a nearly homogeneous lifetime distribution in the beads. As one pixel in the image corresponds to about 0.3 μm in the specimen, one pixel (on average) corresponds to fluorescence originating from a volume of about 0.3×10^{-15} L. As we could not observe defocusing effects of the intensifier by the gain modulation at frequencies from 40–240 MHz (not shown), we estimate the spatial (x–y) resolution to be <400 nm based on the >25 line-pairs/mm resolution of the image intensifier, as specified by Hamamatsu. This is close to the diffraction limit and hence not very different from any standard (non-time-resolved) fluorescence microscopy system.

Concluding Remarks

We have shown the construction and characteristics of a frequency-domain FLIM system. In our opinion, the very accurate lifetime determination and high spatial resolution attainable with this instrument are due to the combination of (i) solving the laser speckle problem by the light scrambling device, (ii) the high modulation depths of the image intensifier and the AOMs used, (iii) the high phase and frequency stability of the instrument, (iv) the minimization of optical components in the emission path, (v) the high sensitivity and gain in the detection devices, (vi) the use of the homodyne method of

detection preventing unnecessary exposure of the sample to excitation light as necessary in many heterodyne implementations (also minimizing photobleaching in the object), and (vi) the near-absence of defocusing and iris effects in the image intensifier.

A specific advantage of frequency-domain FLIM is that no matter how complex the decay of the system may be (i.e., irrespective of K), a simple average lifetime can always be calculated and displayed in images. If necessary, these lifetimes can still be quantitatively related to the individual decaying components [see Eqs. (1) and (2)]. It is of note that the only instrument-dependent parameter in these equations is the frequency of modulation of the detector device. One can prove that irrespective of the actual time-dependent profiles (or shapes) of excitation and detector modulation, these equations are valid provided that one analyzes only the fundamental sine wave of the Fourier spectrum of the detected signal.[33,37] It is of note that for time-domain FLIM, the determined average lifetimes in case of a non-single-exponential decay are dependent on (i) the time-dependent profiles of the pulsed excitation, (ii) the rise and fall characteristics of the applied time gates on the detector, and (iii) the exact time difference and width of the applied time gates or windows of the detector. These three parameters are very much dependent on the type of devices used in the FLIM system and, in principle, are not compatible among different instruments. Therefore, we think that in practice for quantitative studies, frequency-domain FLIM has specific advantages over time-domain FLIM, despite the fact that in theory they are equal (the Fourier transform of one another). On the other hand, time-domain FLIM can have specific advantages in obtaining a high image contrast for slower-decaying components using a late time window,[2,12] as also described for phosphorescence microscopy.[38]

Currently we are applying this FLIM system for measuring molecular interactions in single living cells, for studying receptor–ligand interactions in living plant root systems, and for new ways of imaging *in vivo* cellular indicators for heavy metals and oxygen (Gadella *et al.*, manuscripts in preparation), part of which is also under investigation by others (see accompanying papers and introduction).

ACKNOWLEDGMENTS

We gratefully acknowledge the collaboration with Dr. R. M. Clegg and Dr. T. M. Jovin (Department of Molecular Biology, Max Planck Institute for Biophysical Chemistry, Göttingen, Germany), which was essential for the construction of the FLIM system in our laboratory. This collaboration was supported by the NATO collaborative research grant "Time-Resolved Fluorescence in Solution and in the Microscope." We are grateful to J. de Zwart and J. Goedhart (undergraduate students at the Biochemistry Department at WAU), to F. Vergeldt (Department of Molecular Physics, WAU), and to P. Verveer (Department of Molecular Biology, Max Planck Institute for Biophysical Chemistry) for their assistance in implementing SCIL-Image at the Biochemistry Department in Wageningen. T.W.J.G. was supported by the Foundation for LifeSciences (S.L.W.), which is part of the Dutch Organization for Scientific Research (NWO). The FLIM system described in Fig. 1 was financed by an NWO investment grant awarded to A.J.W.G.V.

REFERENCES

1. B. M. Gadella, M. Lopes-Gardozo, B. Colenbrander, L. M. G. van Golde, and T. W. J. Gadella Jr. (1995) *J. Cell Sci.* **108**, 935–945.
2. R. Cubeddu, G. Canti, P. Taroni, and G. Valentini (1993) *Photochem. Photobiol.* **57**, 480–485.
3. R. Sanders, H. C. Gerritsen, A. Draaier, P. M. Houpt, and Y. K. Levine (1995) *Anal. Biochem.* **227**, 302–308.
4. J. Carrero, T. French, and E. Gratton (1992) *Biophys. J.* **61**, A177.
5. J. R. Lakowicz, H. Szmacinski, K. Nowaczyk, and M. L. Johnson (1992) *Cell Calcium* **13**, 131–147.
6. R. Sanders, H. C. Gerritsen, A. Draaier, P. M. Houpt, and Y. K. Levine (1994) *Bioimaging* **2**, 131–138.
7. T. W. J. Gadella Jr. and T. M. Jovin (1995) *J. Cell Biol.* **129**, 1543–1558.
8. T. Minami and S. Hirayama (1990) *J. Photochem. Photobiol. A Chem.* **53**, 11–21.
9. R. Cubeddu, G. Canti, P. Taroni, and G. Valentini (1991) *Proc. SPIE* **1525**, 17–25.
10. T. Ni and L. Melton (1991) *Appl. Spectrosc.* **45**, 938–943.
11. X. F. Wang, T. Uchida, D. M. Coleman, and S. Minami (1991) *Appl. Spectrosc.* **45**, 360–366.
12. E. P. Buurman, R. Sanders, A. Draaijer, H. C. Gerritsen, J. J. F. van Deen, P. M. Houpt, and Y. K. Levine (1992) *Scanning* **14**, 155–159.
13. M. Kohl, J. Neukammer, U. Sukowski, H. Rinneberg, D. Wörle, H.-J. Sinn, and E. A. Friedrich (1993) *Appl. Phys. B* **56**, 131–138.
14. T. Oida, Y. Sako, and A. Kusumi (1993) *Biophys. J.* **64**, 676–685.
15. H. Schneckenburger, K. König, K. Kunzi-Rapp, C. Westphal-Frösch, and A. Rück (1993) *J. Photochem. Photobiol.* **B21**, 143–147.
16. X. F. Wang, T. Uchida, and S. Minami (1989) *Appl. Spectrosc.* **43**, 840–845.
17. R. M. Clegg, G. Marriott, B. A. Feddersen, E. Gratton, and T. M. Jovin (1990) *Biophys. J.* **57**, 375a.
18. E. Gratton, B. Feddersen, and M. van de Ven (1990) *Proc. SPIE* **1204**, 21–25.
19. C. G. Morgan, A. C. Mitchell, and J. G. Murray (1990) *Trans. R. Microsc. Soc.* **1**, 463–466.
20. J. R. Lakowicz and K. W. Berndt (1991) *Rev. Sci. Instrum.* **62**, 1727–1734.

21. R. M. Clegg, B. Feddersen, E. Gratton, and T. M. Jovin (1992) *Proc. SPIE* **1604**, 448–460.
22. D. W. Piston, D. R. Sandison, and W. W. Webb (1992) *Proc. SPIE* **1604**, 379–389.
23. B. J. Venetta (1959) *Rev. Sci. Instrum.* **30**, 450–457.
24. P. T. C. So, T. French, W. M. Yu, K. M. Berland, C. Y. Dong, and E. Gratton (1995) *Bioimaging* **3**, 49–63.
25. T. W. J. Gadella Jr., T. M. Jovin, and R. M. Clegg (1993) *Biophys. Chem.* **48**, 221–239.
26. M. Van de Ven and E. Gratton (1993) in B. Herman and J. J. Lemasters (Eds.), *Optical Microscopy: Emerging Methods and Applications*, Academic Press, New York, pp. 373–402.
27. H. Szmacinski, J. R. Lakowicz, and M. L. Johnson (1994) *Methods Enzymol.* **240**, 723–748.
28. R. D. Spencer and G. Weber (1969) *Ann. N.Y. Acad. Sci.* **158**, 361–376.
29. G. Weber (1981) *J. Phys. Chem.* **85**, 949–953.
30. D. M. Jameson, E. Gratton, and R. D. Hall (1984) *Appl. Spectrosc. Rev.* **20**, 55–106.
31. T. W. J. Gadella Jr., R. M. Clegg, and T. M. Jovin (1994) *Bioimaging* **2**, 139–159.
32. J. R. Lakowicz, H. S. Szmacinski, K. Nowaczyk, K. W. Berndt, and M. Johnson (1992) *Anal. Biochem.* **202**, 316–330.
33. R. M. Clegg, T. W. J. Gadella Jr., and T. M. Jovin (1994) *Proc. SPIE* **2137**, 105–118.
34. P. T. So, T. French, and E. Gratton (1994) *Proc. SPIE* **2137**, 83–92.
35. A. H. Westphal and A. de Kok (1988) *Eur. J. Biochem.* **172**, 299–305.
36. P. I. H. Bastiaens, A. van Hoek, W. F. Wolkers, J. C. Brochon, and A. J. W. G. Visser (1992) *Biochemistry* **31**, 7050–7060.
37. R. M. Clegg and P. C. Schneider (1996) in J. Slavik (Ed.), *Fluorescence Microscopy and Fluorescence Probes*, Plenum Press, New York, pp. 15–33.
38. G. Marriott, R. M. Clegg, D. J. Arndt-Jovin, and T. M. Jovin (1991) *Biophys. J.* **60**, 1374–1387.